PAPER

Comparison of minimum-norm estimation and beamforming in electrocardiography with acute ischemia

IOP Publishing | Institute of Physics and Engineering in Medicine Physiological Measurement

Physiol. Meas. **35** (2014) 623–638 doi:10.1088/0967-3334/35/4/623

Comparison of minimum-norm estimation and beamforming in electrocardiography with acute ischemia

Teijo Konttila[1], **Ville Mäntynen**[1,2] **and Matti Stenroos**[1]

[1] Department of Biomedical Engineering and Computational Science, Aalto University, Espoo, Finland
[2] BioMag Laboratory, HUS Medical Imaging Center, Helsinki, Finland

E-mail: Teijo.Konttila@aalto.fi

Received 4 September 2013, revised 6 February 2014
Accepted for publication 14 February 2014
Published 12 March 2014

Abstract

In the electrocardiographic (ECG) inverse problem, the electrical activity of the heart is estimated from measured electrocardiogram. A model of thorax conductivities and a model of the cardiac generator is required for the ECG inverse problem. Limitations and errors in methods, models, and data will lead to errors in the estimates. However, in experimental applications, the use of limited or erroneous models is often inevitable due to necessary model simplifications and the difficulty of obtaining accurate 3D anatomical imaging data. In this work, we focus on two methods for solving the inverse problem of ECG in the case of acute ischemia: minimum-norm (MN) estimation and linearly constrained minimum-variance beamforming. We study how these methods perform with different sizes of ischemia and with erroneous conductivity models. The results indicate that the beamformer can localize small ischemia given an accurate model, but it cannot be used for estimating the size of ischemia. The MN estimator is tolerant to geometry errors and excels in estimating the size of ischemia, although the beamformer performs better with accurate model and small ischemia.

Keywords: ECG, body surface potential mapping, ischemia, inverse problem, beamforming, minimum-norm estimate

(Some figures may appear in colour only in the online journal)

1. Introduction

Electrocardiography (ECG) measures voltages of the electric field caused by electrochemical reactions in the heart. ECG is measured non-invasively with electrodes on the body surface.

Thus, in addition to the cardiac electrical activity, the ECG is influenced by the conductivity distribution of the body. In body surface potential mapping (BSPM), ECG is measured with tens of electrodes distributed around the thorax. BSPM can thus be interpreted as the potential distribution on the body surface, and thus we can utilize mathematical modeling in the interpretation of BSPM data.

Myocardial ischemia influences electrochemical reactions in the affected region of the heart, and therefore it may also be seen as changes in the ECG. Ischemia is a result of diminished blood flow to a region of the heart, usually as a result of narrowing or blockage of a coronary artery. The most severe ischemic changes in ECG are detected during a sudden complete obstruction of an artery. Although QRS changes can be present in ischemic ECG, the first signs of ischemia are usually detected in the ST segment or T wave of ECG; T-wave changes are often associated with mild ischemia and ST changes with severe ischemia. These changes are not permanent, and gradually the ST change is reduced as the ischemic area heals or becomes necrotic. If necrosis and eventually scar tissue forms in the injured area, ECG changes may be seen in the QRS complex (Katz 1992).

During ischemia, the action potential of the affected myocardial cells changes (Carmeliet 1999). The severity of ischemia depends on the time from the start of occlusion, the amount of perfusion through the affected or collateral arteries, and the energy demand of the myocardial cells. The changes in the ST segment are mainly caused by the decrease of the resting-state and plateau-state amplitudes of the action potential. When studying the ST-segment changes, ischemia can thus be simulated by decreasing the action potential amplitude in the ischemic region.

The forward problem of ECG deals with determining the ECG from a known source. To solve this problem, a model of body surfaces and conductivities (*a volume conductor model*) is needed. In addition, a computational model for the source of cardiac electrical activity is set up; in this *source model*, the location and type of the sources is modeled, constraining the source distribution to a limited volume, surface, or a point. Due to the complexity of the geometries involved, the forward problem is usually solved using numerical methods with discretized geometries and source models.

1.1. Inverse problem

In the ECG inverse problem, the electrical activity of the heart is estimated from the measured ECG. The inverse problem of ECG is ill-posed, which makes the problem challenging; in order to reach usable source estimates, the problem needs to be constrained to answer a specific question—in this work, we focus on the source of ST-segment changes during ischemia.

3D anatomical imaging of the thorax (e.g. with magnetic resonance imaging) and increasing computing power have allowed the development of methods for non-invasive functional imaging of the heart with ECG. These ECG imaging methods can be divided in two categories: those estimating the activation sequence of the heart (Huiskamp and Greensite 1997, Yamashita 1982, Tilg *et al* 2002, Berger *et al* 2006), and those estimating the epicardial potential (Oster and Rudy 1992, Oster *et al* 1997, 1998, Stenroos and Haueisen 2008). Other approaches include three-dimensional activation imaging (Li and He 2001, He *et al* 2003) and current-density estimation (Lai *et al* 2011).

Methods for solving the inverse problem of ECG have been developed for decades; validations have been carried out with simulations and measurements (e.g., MacLeod and Brooks 1998, van Oosterom 2012, Barr *et al* 1977, Horáček and Clements 1997, Cheng *et al* 2003a, Han *et al* 2011, 2012), and the effect of model errors on estimates has been studied, e.g., in Jiang *et al* (2009), Cheng *et al* (2003b), Messinger-Rapport and Rudy (1986). Inverse

studies of acute ischemia have been done previously (MacLeod *et al* 1995, Li and He 2004, Stenroos *et al* 2005, Nielsen *et al* 2013, Wang *et al* 2013). But to our knowledge, the effect of the location of ischemia on the accuracy of its estimates has not been extensively studied.

Two source estimation methods are used in this work: minimum-norm (MN) estimation (Hämäläinen and Ilmoniemi 1994) and linearly constrained minimum-variance (LCMV) beamforming (Van Veen *et al* 1997). MN estimation is commonly-used approach that reconstructs the measured data with minimum-energy source distribution, and the beamformer is a spatial filter that attempts to evaluate the contribution of each source element to the measured data. Beamforming is frequently applied, e.g., in studies of the brain (Hillebrand *et al* 2005). It has also been applied to magnetocardiographic assessment of atrial arrhythmias (Kim *et al* 2007) but, to our knowledge, its applicability to ECG has not been evaluated. Both approaches need a volume conductor model, and therefore errors in the conductivity profile will also result in errors in the source estimates.

1.2. Task definition

In this work, we evaluate the performance of beamforming and MN estimation in ischemia localization and in estimating the size of the ischemia. We evaluate the source estimation methods globally with ischemia centered on all ventricular vertices. To illustrate the robustness of the methods to errors, we simulate ECG with one thorax geometry and compute the source estimates with two other geometries. This also gives an estimate of errors we should expect in experimental source-estimation scenarios, where individual volume conductor models are not available or contain errors due to, e.g., simplifications and poorly-known conductivities.

2. Models and methods

Computer models were used for comparing the source estimation methods: BSPM data was simulated with ECGSIM[3] software (van Oosterom 2001) and in-house Matlab[4] tools, and source estimation was performed with Matlab functions. In this section, we present the conductivity models, computational methods, and error measures used in this work.

2.1. Conductivity model

Computations were carried out using the anatomical surface models of human thoraces, shown in figure 1. The *reference geometry* (normal young male, NYM) is freely available with the ECGSIM software. It contains lungs (552 vertices) and ventricular compartments (1500 vertices). Two test geometries were created from the reference geometry by changing the thorax surface to that of the Dalhousie thorax (Horáček and Clements 1997) (*test geometry 1*) and to that of a normal male thorax, also available in the ECGSIM software (*test geometry 2*). Electrode positions of the Helsinki 123-lead BSPM layout were projected to the thorax surfaces from our default Dalhousie thorax mesh. The conductivities of the ventricles, lungs, and thorax were assumed as $[1\ 1/4\ 1] \times 0.230\ \mathrm{S\,m^{-1}}$.

2.2. Forward computation

Primary-current distribution $\vec{J}_\mathrm{p}$ was used as source model for myocardial electrical activity (e.g. Gulrajani 1998). The source was represented by a normally oriented primary-current

[3] www.ecgsim.org
[4] www.mathworks.com

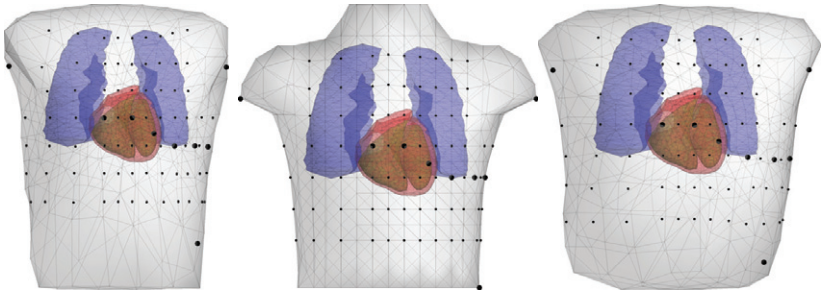

Figure 1. Thorax geometries. (A) reference geometry, (B) test geometry 1, and (C) test geometry 2. All thorax geometries are modified to contain the same source mesh. The large black dots mark the locations of the 12-lead ECG electrodes, and the small black dots mark the locations of the BSPM electrodes.

distribution spanned on the ventricular surface (a so-called double-layer source). The primary current was discretized into N components using linear basis functions centered on each of the N vertices of the ventricular mesh (Stenroos 2008). Transfer matrices were built for each model geometry using linear Galerkin boundary element method (BEM) (Stenroos *et al* 2007, Stenroos and Haueisen 2008, Mosher *et al* 1999), and the potential was interpolated linearly to the M electrode positions using the BEM basis functions. Body surface potential distribution generated by each component i was computed to a lead vector $\boldsymbol{l}_i$, and a lead-field matrix was constructed by combining all N lead vectors to $\boldsymbol{L} = [\boldsymbol{l}_1 \boldsymbol{l}_2 \cdots \boldsymbol{l}_N]$. The surface potential $\boldsymbol{\phi}$ is then computed at M electrodes with

$$\boldsymbol{\phi} = \boldsymbol{L}\boldsymbol{s}, \tag{1}$$

where the source $\boldsymbol{s}$ represents the strength of the primary current at each vertex.

2.3. Simulated data

ECGSIM is a surface-based interactive ECG simulation tool that generates realistic ECG patterns (van Oosterom 2001, van Oosterom and Oostendorp 2004). The source model in ECGSIM is formulated as a double-layer spanned on endo- and epicardial surfaces (Geselowitz 1989), with double-layer amplitude proportional to the amplitude of action potential. The ECGSIM source description can therefore be used with the forward model presented above. Action potential amplitudes for normal activation of the NYM ventricles were imported from ECGSIM to Matlab, where they were used for simulating BSPM signals with roughly circular ischemic regions centered around each ventricular node separately. For each vertex, ischemic regions (*true ischemias*) were defined according to the triangulation; vertices within the radius of each ischemia region were considered ischemic. The effects of ischemia were simulated by decreasing the amplitude of action potential at ischemic vertices by 20%. A reasonable amount of noisy data is needed for inverting the covariance matrix in the beamformer estimator; ten identical ST segments were simulated for each ischemia location and size, and white noise $\boldsymbol{v}$ with 26.5 μV standard deviation (estimated from existing BSPM measurement) was added to the simulated ST segments.

2.4. Source estimation

The source estimates $\hat{\boldsymbol{s}}$ were computed with a linear inverse mapping (source estimator) of the measurement model

$$\hat{\boldsymbol{s}} = \boldsymbol{G}\boldsymbol{\phi} = \boldsymbol{G}(\boldsymbol{L}\boldsymbol{s} + \boldsymbol{v}),$$

where $\boldsymbol{G}$ is the source estimator.

LCMV beamformer is a spatial filter that operates in the source domain; all BSPM signals are projected to the source location i with weight vector $\boldsymbol{w}_i$ by

$$\hat{s}_{\mathrm{BF},i} = \boldsymbol{w}_i^T \boldsymbol{\phi}.$$

The weight vector of LCMV beamformer is optimized to produce minimum variance for this source location, with linear constraint for the corresponding lead vector $\boldsymbol{l}_i$ forcing the output for this lead vector to unity. The minimization problem for the LCMV beamformer is thus

$$\arg\min_{\boldsymbol{w}_i} \left\{ \boldsymbol{w}_i^T \boldsymbol{S} \boldsymbol{w}_i \right\} \quad \text{subject to} \quad \boldsymbol{w}_i^T \boldsymbol{l}_i = 1,$$

where $\boldsymbol{S}$ is the signal moment matrix; typically $\boldsymbol{S}$ is the signal covariance matrix, but the signal moment matrix can be used if the signal is assumed nearly static (Van Veen *et al* 1997). The solution to this minimization problem is (Van Veen *et al* 1997)

$$\boldsymbol{w}_i = \frac{\boldsymbol{S}^{-1}\boldsymbol{l}_i}{\boldsymbol{l}_i^T \boldsymbol{S}^{-1} \boldsymbol{l}_i},$$

and the estimator $\boldsymbol{G}_{\mathrm{BF}}$ for all sources is formed from these vectors by

$$\boldsymbol{G}_{\mathrm{BF}} = [\boldsymbol{w}_1 \boldsymbol{w}_2 \cdots \boldsymbol{w}_{\mathrm{N}}]^T.$$

MN estimate (Hämäläinen and Ilmoniemi 1994) is a solution to the inverse problem that minimizes the ℓ_2-norm of the source estimate. The MN estimator is

$$\boldsymbol{G}_{\mathrm{MN}} = \boldsymbol{L}^T (\boldsymbol{L}\boldsymbol{L}^T + \lambda^2 \boldsymbol{C})^{-1},$$

where λ is the regularization parameter used for weighting between the solution accuracy and noise suppression, and $\boldsymbol{C}$ is the noise covariance matrix. In this work, λ^2 is selected as suggested by Lin *et al* (2006), with an estimated signal-to-noise ratio of 9.

2.5. Metrics

New metrics were defined for comparing the source estimation methods. The localization error (LE) and the accuracy of ischemia extent estimation were determined for ischemia centered on all ventricular nodes separately. The maximum relative amplitude of the estimate as a function of distance from the center of the true ischemia was also plotted to evaluate the estimation of the ischemic region.

LE is the distance from the center of the true ischemia to the center of the best-matching template ischemic region: a template region with the radius of the true ischemia was created for each vertex of the ventricular surface, and the best match was determined by the highest correlation between the estimate and the template region. The definition of LE is illustrated in figure 2.

Extent estimation accuracy (EA) is the ℓ_2-norm of the estimate within the ischemic region normalized by the ℓ_2-norm of the whole estimate. To reduce the effect of LE of EA, the template ischemic region was centered at the best-correlation vertex determined with LE (see figure 2).

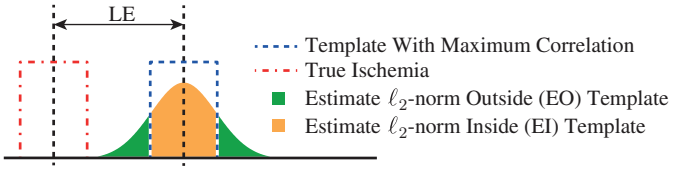

Figure 2. Schematic of the error measures. Localization error (LE) is the distance from the center of the true ischemia to the center of the template region with maximum correlation with the estimate. Extent estimation accuracy (EA) is the ratio of EI and EI+EO.

Maximum amplitude at distance (MD) is the maximum relative amplitude of the source estimate as a function of distance from the center of true ischemia. The distance from the center vertex of the true ischemia was divided into 0.25 cm steps, and the value of each of these steps was set to the maximum relative amplitude of the estimate within that step.

3. Computation and results

We simulated ten beats of BSPM and 12-lead ECG signals with 1 cm (*small ischemia*) and 3 cm (*large ischemia*) radius circular ischemic regions, centered on each of the 1500 epi- and endocardial vertices separately. We defined the ischemic regions according to the distance along the surface from the center vertex; vertices closer than the radius to the center vertex were defined ischemic. From the BSPM simulations we computed the source estimates for the ST segment of the ten beats and computed the average of the estimates for each vertex; we selected the ST segment at the time points between 110–180 ms. For the beamformer, we computed the signal moment matrix $\boldsymbol{S}$ from the ten ST segments.

All ECG simulations were carried out in the reference geometry. The source estimates were computed in the reference geometry and test geometries, shown in figure 1. Due to the similarity of the results in the test geometries, we focus on test geometry 2.

3.1. Example: ischemia simulation and source estimation

First, we present two examples that illustrate the process of ECG simulation and source estimation used in this work. These example simulations, illustrated in the second row of figure 3, show the ST-segment changes caused by ischemia: epicardial ischemia located in the anterior region causes elevation of the ST segment in anterior leads, and endocardial ischemia located in the right lateral region causes ST-segment depression in the right-side lateral leads. For the large endocardial ischemia, the left lateral (and some of the anterior) leads also show ST-segment elevation, which can lead to mislocalization if the spatial coverage of the ECG leads is insufficient.

We then computed the source estimates for the example simulations. In the reference geometry, the peak of the estimates is within the true ischemic region for both ischemia sizes. However, the shape of ischemia is not estimated as accurately as the location: the small-ischemia MN estimate peak is wide and the peak of the large-ischemia beamformer (BF) estimate is narrow compared to the true ischemia. The small-ischemia BF estimate and large-ischemia MN estimate are good approximations of the source in these example cases. As a result of using the test geometries, the shape and location of the peak of the estimate shifts; there is a distinct increase in LE, but the main features seen in the reference geometry remain.

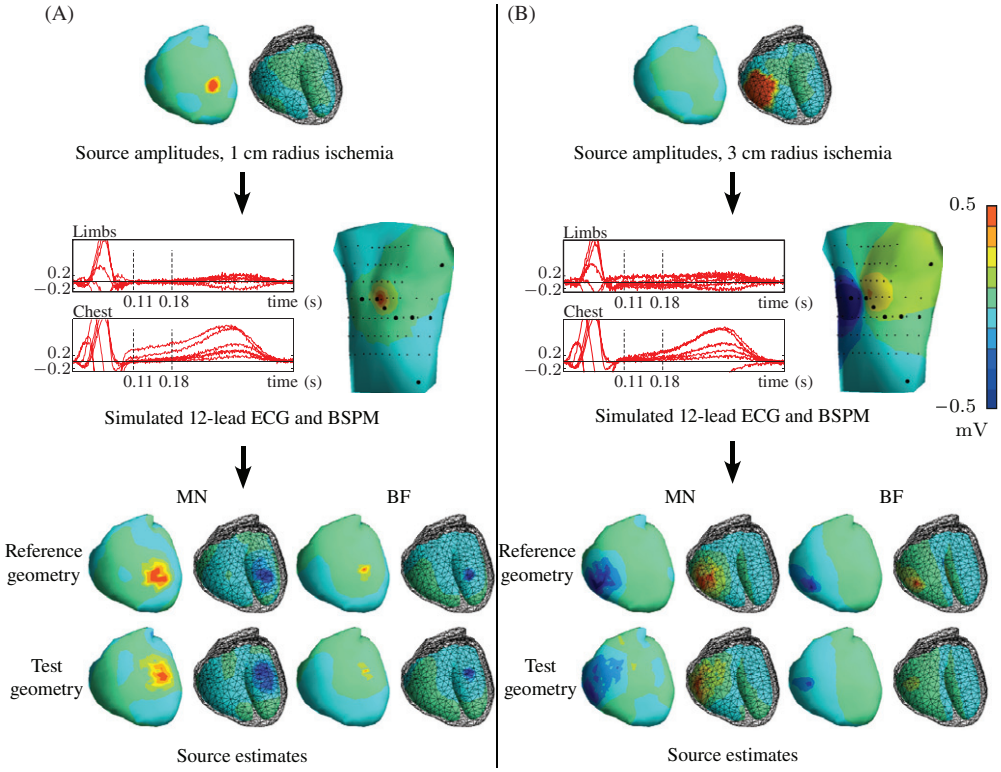

Figure 3. Source estimation with small epicardial ischemia (A) and large endocardial ischemia (B). The example sources shown in the first row are average source amplitudes during the ST segment. Each ventricular plot is divided to a pair of images: the image on the left represents the epicardial surface and the image on the right represents the endocardial surface. Resulting 12-lead ECG and an average BSPM of the ST segment are shown in the second row. The ST-segment time interval used for the source estimation is shown with dashed line with the simulated 12-lead ECG. The scale on the colorbar is for the thorax surface plots, and the plots on the heart surface are scaled to the maximum value of each plot. Source estimates are computed with beamformer (BF) and minimum-norm (MN) estimators in the reference geometry and the test geometry 2 (test geometry). All simulations are carried out with the reference geometry.

Both example estimates leak across the myocardium: the positive peak at the epicardium (endocardium) is accompanied by a negative peak on the endocardium (epicardium). This feature is present in the estimates of both methods and may limit the usefulness of the endocardial surfaces in source estimation (the role of endocardial surface is studied further later in this section). Next, we evaluate the estimators with the metrics of section 2.5 for ischemia centered on all ventricular vertices.

3.2. Localization error

LEs with the reference geometry and test geometry 2 are shown in figure 4. The small ischemic regions are localized with both methods and the LEs for the beamformer are lower. The methods perform in a similar way as in the example shown in section 3.1: the LEs of large ischemic regions are smaller for MN estimator and the LEs of small ischemias are lower for beamforming. Mean LEs are shown in table 1.

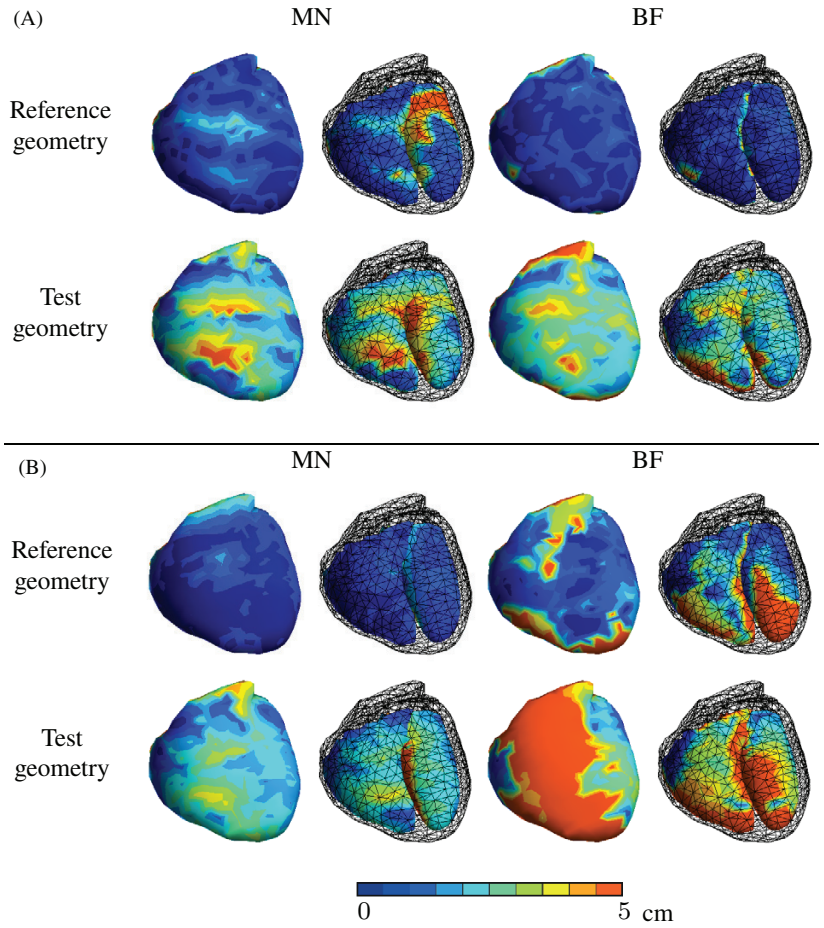

Figure 4. Localization error (LE) for small ischemia (A) and large ischemia (B). The amplitude at each node represents the localization error for ischemia centered around that node. For further details, see the caption of figure 3.

The introduction of geometry errors increases LEs, but the performance of the methods remains similar: the beamformer remains better for localizing small ischemia, but the MN estimator is not far behind. However, in the erroneous test geometries, the beamforming cannot reliably localize large ischemias: LEs are above 5 cm for most of the epicardial surface. The septum is sensitive to geometry errors and shows increased errors for the MN estimates of small ischemia and the BF estimates of large ischemia.

3.3. Extent estimation accuracy

Extent estimation accuracy (EA) with the reference geometry and test geometry 2 are shown in figure 5. The EA of beamforming for both ischemia sizes shows spots with good EA. However, the EA is dependent on the location of ischemia, and therefore beamforming is not a reliable method for ischemia extent estimation. MN estimator cannot estimate the size of small ischemia, but it has a significant region with above 0.9 EA for large ischemia on epi- and endocardial surfaces.

Table 1. Localization errors (LE) for all geometries (in centimeters). Results are presented separately for epicardial and endocardial surfaces as mean ± standard deviation. The ECG simulations were computed in the reference geometry. Heart 1 is the heart mesh from the reference geometry, and heart 2 is the convex version of the same heart remeshed without the endocardial surface.

Source size Inverse geometries	MN endo	MN epi	BF endo	BF epi
1 cm source				
Heart 1, reference geometry	3.4 ± 2.4	1.9 ± 2.4	1.0 ± 1.3	0.9 ± 1.3
Heart 1, test geometry 1	4.0 ± 2.1	3.2 ± 2.8	3.2 ± 2.3	2.8 ± 2.0
Heart 1, test geometry 2	3.8 ± 2.2	3.3 ± 3.0	3.3 ± 2.3	2.8 ± 2.1
Heart 2, reference geometry	3.4 ± 2.4	2.0 ± 2.2	3.3 ± 2.8	1.0 ± 1.4
Heart 2, test geometry 1	4.3 ± 2.2	3.1 ± 2.6	4.6 ± 3.0	2.9 ± 2.7
Heart 2, test geometry 2	3.9 ± 2.3	3.1 ± 2.8	4.4 ± 2.7	3.5 ± 3.1
3 cm source				
Heart 1, reference geometry	1.6 ± 1.4	0.7 ± 0.6	2.3 ± 2.1	1.8 ± 2.3
Heart 1, test geometry 1	2.6 ± 1.6	1.9 ± 1.0	3.5 ± 2.6	4.1 ± 3.1
Heart 1, test geometry 2	2.8 ± 1.8	1.9 ± 0.9	4.0 ± 2.5	4.5 ± 3.3
Heart 2, reference geometry	2.3 ± 1.7	0.7 ± 0.4	4.2 ± 2.8	1.7 ± 2.5
Heart 2, test geometry 1	3.3 ± 1.8	2.0 ± 0.8	5.3 ± 3.0	4.4 ± 3.8
Heart 2, test geometry 2	3.4 ± 2.0	2.0 ± 0.8	5.1 ± 3.0	4.9 ± 3.9

When the test geometries are used for source estimation, the resulting estimates shift (see the examples shown in section 3.1) which makes the extent estimation less accurate. Otherwise the EA distribution computed in the test geometry 2 is similar to that computed in the reference geometry.

3.4. Ischemia size estimation with minimum-norm estimator

Ischemia size estimation with the MN estimator seemed promising. To further study the ability of MN estimation to characterize ischemia, we used the maximum amplitude at distance (MD) metric; we plotted the shape of the estimate distribution as a function of distance from the center vertex. We simulated ischemia with 1–6 cm radius, centered on all vertices separately, and then computed the mean and standard deviation of MD for each ischemia size, shown in figure 6. The shape of the distribution does not change much from 1 to 3 cm source radius, although the distribution for the smallest ischemia is slightly worse; both the standard deviation and the mean of MD outside the true ischemia are higher with the 1 cm radius ischemia than the larger ischemias. Above 3 cm radius the peak starts extending with the true ischemic region, which indicates that the MN estimator gives a good estimate for the extent of sources with radius of 3 cm and larger.

3.5. The role of endocardial surface

If ischemia localization is based on amplitude, the majority of the endocardial ischemic regions are localized on the epicardium, including the examples in figure 3. In these example cases, the amplitude near the true ischemic site is higher on the epicardial surface for both ischemia locations, but the sign of the estimate helps identify the true ischemic surface. To further study the significance of the endocardial surface in source estimation, we created a convex version of the ventricular meshes (*convex geometry*) of the reference geometry with iso2mesh[5] (Fang

[5] iso2mesh.sf.net

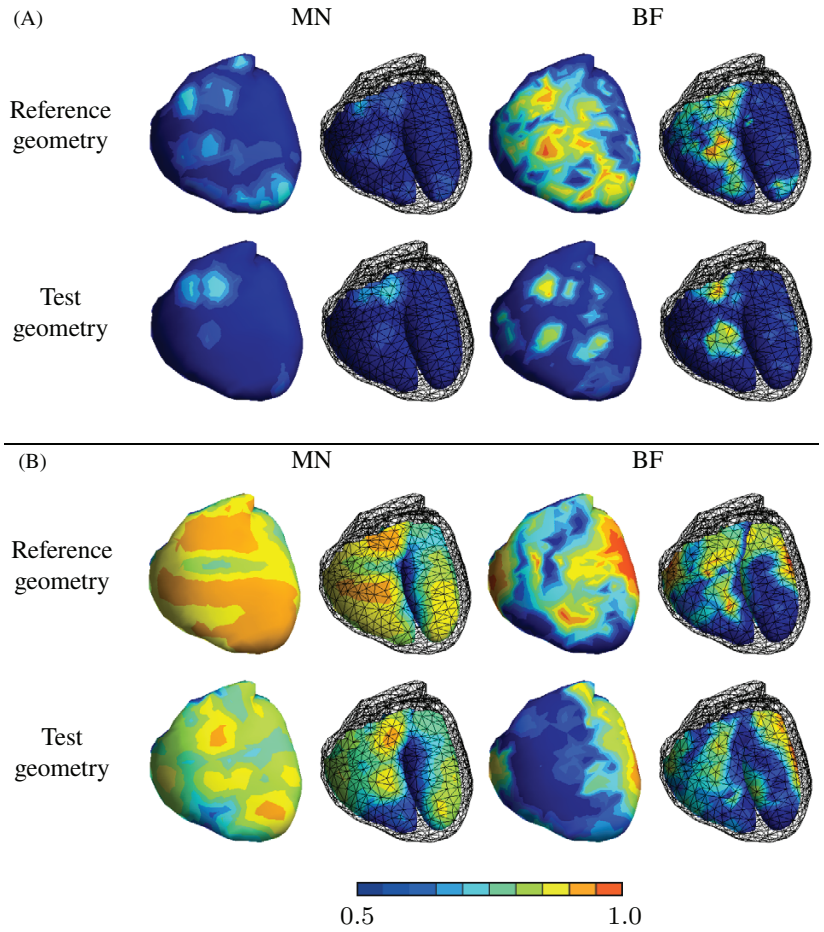

Figure 5. Extent estimation accuracy (EA) for small ischemia (A) and large ischemia (B). The amplitude at each vertex represents the accuracy of extent estimation for ischemia centered around that vertex. For further details, see the caption of figure 3.

and Boas 2009) Matlab toolbox. The convex geometry contains all surfaces of the reference geometry except the ventricular mesh that is replaced by its convex hull; the source model used in the estimators was thus spanned on the epicardial surface only. We computed the metrics of section 2.5 for the convex geometry. The results are shown in figure A1 in the appendix; they are nearly identical to the results with endocardial surfaces (figures 4–5), and even the endocardial ischemias are estimated with similar accuracy, as shown in table 1. Only the results for the beamformer near the septum are significantly worse without the endocardial surface.

4. Discussion

In this work, we studied the localization and size estimation of acute ischemia. We have previously studied the use of BSPM after myocardial infarction in prediction of myocardial recovery (Kylmälä *et al* 2013), arrhythmic events (Korhonen *et al* 2009), and cardiac deaths (Korhonen *et al* 2010). Those investigations were based on detecting BSPM features in signal

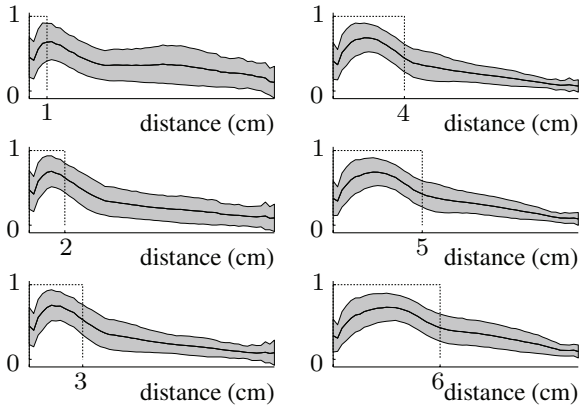

Figure 6. Mean and standard deviation of maximum amplitude at distance (MD) for various sizes of ischemia with minimum-norm (MN) estimate. The dashed black line shows the true ischemia size, black curve represents the mean of the MD computed separately for ischemia centered on all nodes on the ventricular surface, and the gray areas show the standard deviation.

space. However, the interpretation of spatial events is difficult without the incorporation of a volume conductor model. In this work, we projected the BSPM features to the heart surface with two source-estimation approaches and studied how the use of erroneous volume conductor model affects the projections. The signal feature used in this study was the nearly static part of the ST segment. Thus we could use linear source estimation methods and did not need time-domain imaging and nonlinear optimization (Huiskamp and Greensite 1997) or temporal regularization (Oster and Rudy 1992).

4.1. Comparison to previous ischemia studies

We determined the ischemia LE and extent estimation accuracy for all possible sites of ventricular ischemia. This global approach was used in order to gain information on the sensitivity of the measurement setup, and behavior and robustness of the estimators. Our approach thus adds to previously published studies that focus on simulated or measured data during ischemia at a few locations; knowledge obtained with global simulation studies facilitates design of experimental studies and interpretation of clinical results. Essential studies of ischemia localization using BSPM are elaborated below.

Previous work in ischemia detection by MacLeod *et al* (1995) focused on ischemia localization using coronary angioplasty as a model of controlled ischemia; this method completely blocks the blood flow of the artery beyond the inflatable-balloon catheter for up to 120 s. In their investigation, MacLeod *et al* were able to detect the expected ST, STT, and QRST changes in the epicardial potential of seven patients. Later, Stenroos *et al* (2005) used a population of 22 coronary angioplasty patients to successfully localize the ischemia of most of the patients. Both of these investigations were carried out using the Dalhousie thorax and evaluated the ischemia location using the epicardial potential computed from the BSPM determined by subtracting pre-balloon map from the peak balloon-inflation map.

To our knowledge, the first transmural assessment of myocardial ischemia localization was reported by Li and He (2004). They localized simulated ischemia at ten locations using neural networks. Recently, Nielsen *et al* (2013) published an investigation on ischemia localization, describing detailed anisotropic volume conductor model to reconstruct the ischemia in four

patients. Similarly, Wang *et al* (2013) published an optimization framework for transmural ischemia localization with an example case of one simulated ischemia and one animal experiment.

4.2. Models

We used a double-layer spanned on the surface of the heart as a source model for the ECG simulations. These simulations are based on an equivalent surface source model developed by, e.g., van Oosterom (2001). In these simulations, the source strengths were pre-defined in the ECGSIM software (by fitting them to measured data). A drawback of using surface-based models is the inability to include anisotropic conductivities in the forward simulations. However, since the source strengths were defined by fitting them to measured data, the effect of anisotropy is implicitly included in the source strengths.

For the inverse problem, we used the same distributed source model as for the simulations. The choice of source model depends on the problem; in this work, we estimated the primary-current distribution on the heart surface during the ST segment. We utilized a double-layer source model because

- a normally oriented dipole or dipole distribution is a typical equivalent representation for the ischemic source,
- it is an alternative to epicardial potential as suggested by Horáček and Clements (1997),
- the epicardial double-layer is closely related to the epicardial potential of an isolated heart as shown by Geselowitz (1989), and
- it is easier to include complicated conductivity models with the double-layer source model than with the epicardial potential model (Stenroos 2009).

As the model used in this study cannot explicitly take anisotropy into account, the simulations of endocardial ischemia are not as accurate as those of epicardial ischemia. This limits the ability of this forward model to characterize ischemias with different myocardial depths. However, the effects of anisotropy on the location of ST-segment shifts caused by shallow ischemia residing near endocardium have been reported as small in slab simulations (Johnston *et al* 2001). Heart-in-torso simulations suggest that both deeper endocardial and transmural ischemia are also locatable by ST-segment shift above the ischemic region (MacLachlan *et al* 2005) or, depending on the myocardial depth of ischemia, over the lateral boundary between healthy and ischemic tissue (Hopenfeld *et al* 2004).

Ischemia decreases the local conductivity of the affected region: measurements by Kléber and Riegger (1987) indicated that the drop of perfusion pressure can decrease the longitudinal extracellular conductivity by up to 35%. The surface where the primary and surface-equivalent sources are spanned on is also the boundary where the conductivity changes; the influence of this boundary on volume currents can be represented by a double-layer on the boundary. This kind of source/conductivity configuration may influence local current distribution considerably, but the far-field effects are mainly seen in the amplitude of the body surface potentials. We verified this theoretical reasoning with simple simulations, where we varied the conductivity inside a pillbox-shaped ischemia (not shown here), the change of topographies was minimal (correlation between map patterns >0.999 for both 1 and 3 cm ischemia), while the amplitude difference was noticeable (relative errors 7% and 33% for 1 cm and 3 cm ischemia respectively). As our localization measures are based on shapes of the estimated source distribution instead of source amplitudes, we considered it safe to omit the conductivity changes in our simulated ECGs.

4.3. Location-dependence of source estimation

Previous ischemia studies motivated us to carry out an extensive investigation in to the influence of ischemia location on both the localization accuracy and the extent estimation accuracy with BSPM. The estimation of extent influences the choice of treatment in the emergency care: a larger ischemic area requires more aggressive reperfusion treatment. We used two ischemia sizes centered on each node of the ventricular mesh. This allowed us to identify location-dependent weaknesses of the source estimation methods, including the following.

- The localization of ischemia on the septum was difficult. The MN estimator for small ischemic region and beamformer for large ischemic region showed higher LEs at the septum even with the reference geometry, and the errors were emphasized with the use of test geometries (figure 4).
- Localization and extent estimation was consistently easier on the epicardium than the endocardium (figures 4 and 5).
- Distance between the source and the electrodes influenced the accuracy, as shown clearly in the extent estimation accuracy of the MN estimate (figure 5).
- Removal of the endocardial surfaces from source estimation was strongly reflected in the septum in the case of beamformer estimates—the LE for the septum was above 5 cm (figure A1). However, elsewhere the performance did not change much.

4.4. Comparison of minimum-norm estimation and beamformer

The results for LE and size estimation in figures 4 and 5 in the reference geometry showed the main differences between the two methods used in this work: the beamformer estimates were sharply peaked and seemed optimal for localizing point sources, while the MN estimates were smooth and capable of localizing and estimating the extent of larger ischemias. Further tests with various sizes of ischemia showed similar properties: beamforming localizes sources with radius smaller than 2 cm better than MN estimator, while MN localizes larger sources better than beamforming. Localization of small sources with the beamformer was difficult only near the septum, but the localization became more unstable when the size of the ischemia increased. Estimating the size of ischemia was not feasible with the beamformer; it was only possible with sources larger than 3 cm radius using the MN estimator (figure 6).

The inclusion of geometry errors reduced the localization accuracy as expected. Localizing small ischemias with the beamformer was still possible, but it could not be used for localizing larger sources. The beamformer is a promising method for localizing small sources, but it seems sensitive to geometry errors; when the same (or nearly identical) lead field is absent for both inverse and forward computation, the LE is high. This was emphasized when the endocardial surfaces were removed from the inverse computation, resulting in an over 5 cm LE in the septum. The rest of the lead fields of the endocardium have opposite-sign counterparts on the epicardium, and therefore the localization was successful. The inclusion of geometry errors did not cause instability to the MN estimates, although the LE increased significantly; the estimates shifted by approximately 2 cm.

We identified the strengths and weaknesses of both methods in the estimation of ischemic region: the beamformer performs better than the MN estimator with accurate model and small ischemia, and the MN estimator is a robust approach that is tolerant to geometry errors and excels in estimating the size of ischemia. As the computation of linear estimators is fast, it may be beneficial to compute the estimates with both methods. In future work, one potential approach is a spatial filter framework that can be used for combining properties of both methods in one estimator (DeFleCT, Hauk and Stenroos 2014).

Appendix. Inverse computation without endocardial surface

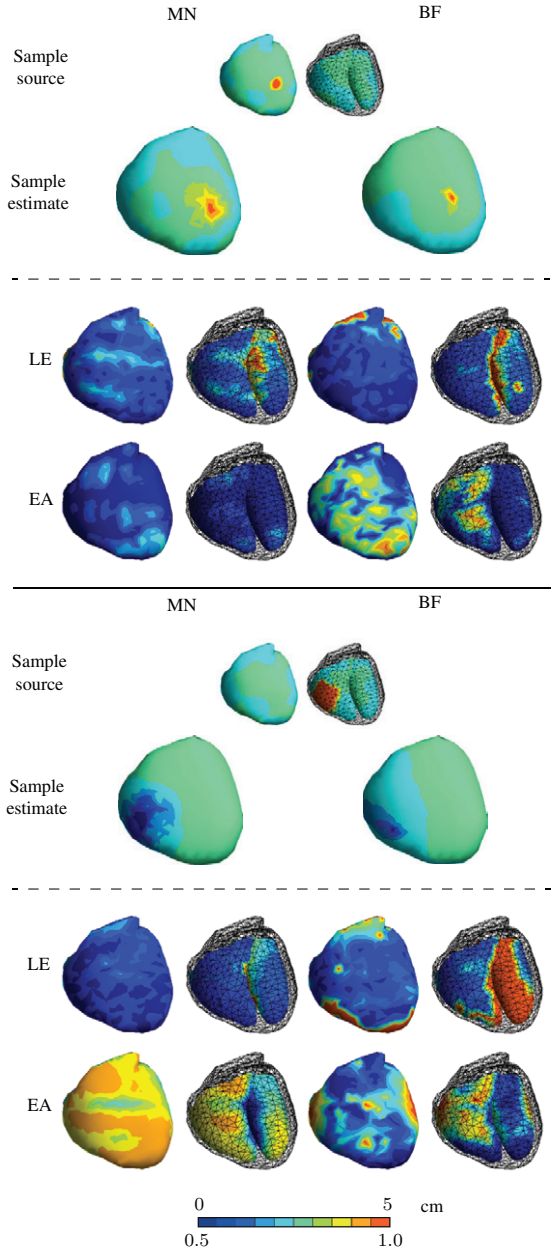

Figure A1. Source estimates and error measures for ischemic ST segment. Source estimation is done without the endocardial mesh. The scale of LE is above the colorbar and the scale of EA is below the colorbar. For further details, see the captions of figures 3–5.

References

Barr R C, Ramsey M and Spach M S 1977 Relating epicardial to body surface potential distributions by means of transfer coefficients based on geometry measurements *IEEE Trans. Biomed. Eng.* **24** 1–11

Berger T *et al* 2006 Single-beat noninvasive imaging of cardiac electrophysiology of ventricular pre-excitation *J. Am. College Cardiol.* **48** 2045–52

Carmeliet E 1999 Cardiac ionic currents and acute ischemia: from channels to arrhythmias *Physiol. Rev.* **79** 917–1017

Cheng L K, Bodley J M and Pullan A J 2003a Comparison of potential- and activation-based formulations for the inverse problem of electrocardiology *IEEE Trans. Biomed. Eng.* **50** 11–22

Cheng L K, Bodley J M and Pullan A J 2003b Effects of experimental and modeling errors on electrocardiographic inverse formulations *IEEE Trans. Biomed. Eng.* **50** 23–32

Fang Q and Boas D A 2009 Tetrahedral mesh generation from volumetric binary and gray-scale images *Proc. IEEE Int. Symp. on Biomedical Imaging* pp 1142–5

Geselowitz D B 1989 On the theory of the electrocardiogram *Proc. IEEE* **77** 857–76

Gulrajani R 1998 *Bioelectricity and Biomagnetism* (New York: Wiley)

Hämäläinen M S and Ilmoniemi R J 1994 Interpreting magnetic fields of the brain: minimum norm estimates *Med. Biol. Eng. Comput.* **32** 35–42

Han C, Pogwizd S M, Killingsworth C R and He B 2011 Noninvasive imaging of three-dimensional cardiac activation sequence during pacing and ventricular tachycardia *Heart Rhythm* **8** 1266–72

Han C, Pogwizd S M, Killingsworth C R and He B 2012 Noninvasive reconstruction of the three-dimensional ventricular activation sequence during pacing and ventricular tachycardia in the canine heart *Am. J. Physiol. Heart Circ. Physiol.* **302** H244–52

Hauk O and Stenroos M 2014 A framework for the design of flexible cross-talk functions for spatial filtering of EEG/MEG data: DeFleCT *Hum. Brain Mapp.* at press (doi: 10.1002/hbm.22279)

He B, Li G and Zhang X 2003 Noninvasive imaging of cardiac transmembrane potentials within three-dimensional myocardium by means of a realistic geometry anisotropic heart model *IEEE Trans. Biomed. Eng.* **50** 1190–202

Hillebrand A, Singh K D, Holliday I E, Furlong P L and Barnes G R 2005 A new approach to neuroimaging with magnetoencephalography *Hum. Brain Mapp.* **25** 199–211

Hopenfeld B, Stinstra J G and Macleod R S 2004 Mechanism for ST depression associated with contiguous subendocardial ischemia *J. Cardiovasc. Electrophysiol.* **15** 1200–6

Horáček B M and Clements J C 1997 The inverse problem of electrocardiography: a solution in terms of single- and double-layer sources of the epicardial surface *Math. Biosci.* **144** 119–54

Huiskamp G and Greensite F 1997 A new method for myocardial activation imaging *IEEE Trans. Biomed. Eng.* **44** 433–46

Jiang M, Xia L, Shou G, Wei Q, Liu F and Crozier S 2009 Effect of cardiac motion on solution of the electrocardiography inverse problem *IEEE Trans. Biomed. Eng.* **56** 923–31

Johnston P R, Kilpatrick D and Li C Y 2001 The importance of anisotropy in modeling ST segment shift in subendocardial ischaemia *IEEE Trans. Biomed. Eng.* **48** 1366–76

Katz A M 1992 *Physiology of the Heart* 2nd edn (New York: Raven Press)

Kim D, Kim K, Lee Y H and Ahn H 2007 Detection of atrial arrhythmia in superconducting quantum interference device magnetocardiography; preliminary result of a totally-noninvasive localization method for atrial current mapping *Interact. Cardiovasc. Thorac. Surg.* **6** 274–9

Kléber A G and Riegger C B 1987 Electrical constants of arterially perfused rabbit papillary muscle *J. Physiol. (Lond.)* **385** 307–24

Korhonen P, Husa T, Konttila T, Tierala I, Mäkijärvi M, Väänänen H, Ojanen J, Vehtari A and Toivonen L 2010 Fragmented QRS in prediction of cardiac deaths and heart failure hospitalizations after myocardial infarction *Ann. Noninvasive Electrocardiol.* **15** 130–7

Korhonen P, Husa T, Konttila T, Tierala I, Mäkijärvi M, Väänänen H and Toivonen L 2009 Complex T-wave morphology in body surface potential mapping in prediction of arrhythmic events in patients with acute myocardial infarction and cardiac dysfunction *Europace* **11** 514–20

Kylmälä M, Konttila T, Vesterinen P, Lindholm M, Nieminen M, Stenroos M, Väänänen H, Hänninen H and Toivonen L 2013 Predicting recovery of myocardial function by electrocardiography after acute infarction *Ann. Noninvasive Electrocardiol.* **18** 230–9

Lai D, Liu C, Eggen M D, Iaizzo P A and He B 2011 Localization of endocardial ectopic activity by means of noninvasive endocardial surface current density reconstruction *Phys. Med. Biol.* **56** 4161–76

Li G and He B 2001 Localization of the site of origin of cardiac activation by means of a heart-model-based electrocardiographic imaging approach *IEEE Trans. Biomed. Eng.* **48** 660–9

Li G and He B 2004 Non-invasive estimation of myocardial infarction by means of a heart-model-based imaging approach: a simulation study *Med. Biol. Eng. Comput.* **42** 128–36

Lin F H, Belliveau J W, Dale A M and Hämäläinen M S 2006 Distributed current estimates using cortical orientation constraints *Hum. Brain Mapp.* **27** 1–13

MacLachlan M C, Sundnes J and Lines G T 2005 Simulation of ST segment changes during subendocardial ischemia using a realistic 3-D cardiac geometry *IEEE Trans. Biomed. Eng.* **52** 799–807

MacLeod R S and Brooks D H 1998 Recent progress in inverse problems in electrocardiology *IEEE Eng. Med. Biol. Mag.* **17** 73–83

MacLeod R S, Gardner M, Miller R M and Horáček B M 1995 Application of an electrocardiographic inverse solution to localize ischemia during coronary angioplasty *J. Cardiovasc. Electrophysiol.* **6** 2–18

Messinger-Rapport B J and Rudy Y 1986 The inverse problem in electrocardiography: a model study of the effects of geometry and conductivity parameters on the reconstruction of epicardial potentials *IEEE Trans. Biomed. Eng.* **33** 667–76

Mosher J C, Leahy R M and Lewis P S 1999 EEG and MEG: forward solutions for inverse methods *IEEE Trans. Biomed. Eng.* **46** 245–59

Nielsen B F, Lysaker M and Grøttum P 2013 Computing ischemic regions in the heart with the bidomain model—first steps towards validation *IEEE Trans. Med. Imaging* **32** 1085–96

Oster H S and Rudy Y 1992 The use of temporal information in the regularization of the inverse problem of electrocardiography *IEEE Trans. Biomed. Eng.* **39** 65–75

Oster H S, Taccardi B, Lux R L, Ershler P R and Rudy Y 1997 Noninvasive electrocardiographic imaging: reconstruction of epicardial potentials, electrograms, and isochrones and localization of single and multiple electrocardiac events *Circulation* **96** 1012–24

Oster H S, Taccardi B, Lux R L, Ershler P R and Rudy Y 1998 Electrocardiographic imaging: noninvasive characterization of intramural myocardial activation from inverse-reconstructed epicardial potentials and electrograms *Circulation* **97** 1496–507

Stenroos M 2008 Boundary element method in spatial characterization of the electrocardiogram *Dissertation for the Degree of Doctor of Science in Technology* Helsinki University of Technology (http://lib.tkk.fi/Diss/2008/ isbn9789512295876/)

Stenroos M 2009 The transfer matrix for epicardial potential in a piece-wise homogeneous thorax model: the boundary element formulation *Phys. Med. Biol.* **54** 5443–55

Stenroos M, Hänninen H, Lindholm M, Tierala I and Katila T 2005 Lead field formulation for epicardial potential in electrocardiographic localization of acute myocardial ischemia *IFMBE Proc.* **11** 2265-1–5

Stenroos M and Haueisen J 2008 Boundary element computations in the forward and inverse problems of electrocardiography: comparison of collocation and Galerkin weightings *IEEE Trans. Biomed. Eng.* **55** 2124–33

Stenroos M, Mäntynen V and Nenonen J 2007 A Matlab library for solving quasi-static volume conduction problems using the boundary element method *Comput. Methods Programs Biomed.* **88** 256–63

Tilg B, Fischer G, Modre R, Hanser F, Messnarz B, Schocke M, Kremser C, Berger T, Hintringer F and Roithinger F X 2002 Model-based imaging of cardiac electrical excitation in humans *IEEE Trans. Med. Imaging* **21** 1031–9

van Oosterom A 2001 Genesis of the T wave as based on an equivalent surface source model *J. Electrocardiol.* **34** 217–27

van Oosterom A 2012 The inverse problem of bioelectricity: an evaluation *Med. Biol. Eng. Comput.* **50** 891–902

van Oosterom A and Oostendorp T F 2004 ECGSIM: an interactive tool for studying the genesis of QRST waveforms *Heart* **90** 165–8

Van Veen B D, van Drongelen W, Yuchtman M and Suzuki A 1997 Localization of brain electrical activity via linearly constrained minimum variance spatial filtering *IEEE Trans. Biomed. Eng.* **44** 867–80

Wang D, Kirby R M, MacLeod R S and Johnson C R 2013 Inverse electrocardiographic source localization of ischemia: an optimization framework and finite element solution *J. Comput. Phys.* **250** 403–24

Yamashita Y 1982 Theoretical studies on the inverse problem in electrocardiography and the uniqueness of the solution *IEEE Trans. Biomed. Eng.* **29** 719–25